Journal of Materials Chemistry B

RSC Publishing

PAPER

View Article Online
View Journal

Cite this: DOI: 10.1039/c3tb21197e

Apoferritin-encapsulated PbS quantum dots significantly inhibit growth of colorectal carcinoma cells

Tracey D. Bradshaw,*[a] Marc Junor,[a] Amalia Patanè,[b] Phil Clarke,[c] Neil R. Thomas,[d] Mei Li,[e] Stephen Mann[e] and Lyudmila Turyanska*[b]

Received 28th August 2013
Accepted 8th October 2013

DOI: 10.1039/c3tb21197e

www.rsc.org/MaterialsB

Colorectal carcinoma (CRC) is the 3rd most common cancer worldwide, thus development of novel therapeutic strategies is imperative. Herein potent, selective dose-dependent antitumor activity of horse spleen apoferritin encapsulated PbS quantum dots (AFt-PbS) against two human-derived colorectal carcinoma cell lines is reported ($GI_{50} \sim 70$ μg mL^{-1}). Following *in vitro* exposure to AFt-PbS, CRC cells fail to recover proliferative capacity, and undergo apoptosis triggered by the generation of reactive oxygen species (ROS). In stark contrast, the AFt-PbS nanocomposites do not affect the growth and cell cycle of non-tumor human microvessel endothelial HMEC-1 cells ($GI_{50} > 500$ μg mL^{-1}). *In vivo*, AFt-PbS QDs are well tolerated by mice. Neither adverse health nor behavioral indicators were observed throughout the 15 day study. The photoluminescence of AFt-PbS combined with selective antitumor activity offer potential development of AFt-PbS for simultaneous non-invasive imaging and treatment of malignant tissue.

Introduction

Colorectal carcinoma (CRC) is the third most common cancer globally, responsible for >600 000 deaths in 2008.[1] The current initial therapeutic approach for colon cancer treatment is surgery. However, 5 year survival remains <50% for both sexes. Adjuvant chemotherapy has an established role in management of CRC, and in rectal cancer radiotherapy is combined with chemotherapy. 5-Fluorouracil (5FU) plus calcium folinate has been a standard chemotherapy treatment for more than 40 years, yet in advanced CRC tumor response rates are typically below 15% with median survival of ~1 year.[2] Clinical trial results[3] clearly demonstrated the beneficial combination of irinotecan, 5FU and calcium folinate that was adopted in 2001 as first line treatment for metastatic CRC.[4] Additional licensed treatments include the platinum analogue oxaliplatin and biological therapies cetuximab (Erbitux) and bevacizumab (Avastin) monoclonal antibodies. Nevertheless, for inoperable, advanced and metastatic CRC, development of novel chemotherapeutic agents remains imperative.

Nanomedicine offers potential to transform treatment and diagnosis of many diseases, including cancer. Indeed more than 40 nanomedical agents have reached the clinic[5] and development of new agents represents a growing area of research.[6,7] As nano-technologies advance, they will play more prominent roles in early cancer detection and intervention. Theranostic agents that combine selective therapy and fluorescence may allow swift development of personalized treatment regimens. Recently, the effects of several nanomaterial systems on CRC have been explored. Metal nanoparticles (Au spheres, rods)[8,9] and $Cu_{2-x}Se$ nanocrystals[23] have been successfully used in photothermal treatment of CRC. For diagnostic and/or treatment applications, nanoparticles with small hydrodynamic diameters are considered preferable as they provide longer blood circulation times. Semiconductor quantum dots (QDs) typically have small diameters (3–10 nm) and possess brighter, more stable photoluminescence (PL) compared to organic dyes. In CRC cells, II–VI QDs (CdSe, ZnS, CdTe) have shown potential as imaging labels,[10] as markers in magnetic immunoassays,[11] and have been developed as biosensors for quantitative pharmacology studies.[12] On the other hand, II–VI QDs have limited applications as self-reporting therapeutic agents, since they emit light in the visible part of the electromagnetic spectrum, where biological tissues have significant absorption. QDs with emission/absorption in the near-infrared (NIR) wavelength range, 1000–1350 nm, are advantageous, offering potential for deep tissue *in vivo* imaging.[13] Encapsulation of a nanoparticle in an apoferritin (AFt) shell allows stealthy transportation and delivery of complex molecular cargoes to diseased, specifically malignant

[a]School of Pharmacy, The University of Nottingham, Nottingham NG7 2RD, UK. E-mail: Tracey.Bradshaw@nottingham.ac.uk
[b]School of Physics and Astronomy, The University of Nottingham, Nottingham NG7 2RD, UK. E-mail: Lyudmila.Turyanska@nottingham.ac.uk
[c]School of Clinical Sciences, The University of Nottingham, Nottingham NG7 2RD, UK
[d]Centre for Biomolecular Sciences, School of Chemistry, The University of Nottingham, Nottingham NG7 2RD, UK
[e]Centre for Organized Matter Chemistry, School of Chemistry, University of Bristol, Bristol BS8 1TS, UK

tissues and addresses challenges associated with drug-related adverse toxicity, bioavailability and resistance.[14–19] AFt binds ferrous iron, forming ferritin, for intracellular iron storage. Cancer cells possess an avid appetite for iron which is transported into cells *via* transferrin receptor (TR)-mediated endocytosis. Consequently, in contrast to the limited expression of TR in normal tissues, TR expression is widely distributed and up-regulated in malignant tissue including CRC.[20–22] To our knowledge, the effect of quantum dots encapsulated in apoferritin on CRC and the *in vivo* toxicity of these nanocomposites were not studied before.

Here we report *in vitro* antitumor activity of NIR light emitting AFt-PbS QDs[25] in human-derived CRC cells HCT116 and HT29. Exposure to AFt-PbS causes selective, dose-dependent growth inhibition of CRC cells and induces apoptotic cell death *via* a mechanism involving generation of reactive oxygen species (ROS). Of great potential is the effect of AFt-PbS on colony formation of CRC cells: even at low exposure concentrations and times ($0.1\times$ GI_{50} for 24 h) the cancerous cells lose the ability to form colonies. Assessment of risk towards normal tissues is examined in non-tumorigenic human microvessel endothelial cells (HMEC-1) where at the same exposure conditions no effects on cell proliferation were observed. *In vivo* acute toxicity study of AFt-PbS in non-tumor and HCT116-tumor-bearing mice revealed no adverse effects over a 15 day period. Further experiments are now required to investigate antitumor efficacy of AFt-PbS *in vivo*.

Results and discussion

PbS QDs were synthesized by colloidal chemistry in aqueous solution. The wavelength of their PL emission is tuneable by the QD diameter from 2 nm to 8 nm (Fig. 1). Details of the nanoparticle synthesis, together with structural and optical properties are reported elsewhere.[19,24–26] Nanoparticles were successfully imaged *in vivo*. The inset of Fig. 1a shows the PL of PbS solution injected within the peritoneal cavity of a mouse cadaver. In this study we used QDs with PL emission in the NIR wavelength range, 1000–1300 nm. PbS QDs were encapsulated within the hollow cavity of horse spleen AFt to facilitate cellular uptake of the nanocrystals. Colloidal AFt-PbS solutions were found to be stable over a period of at least 3 months. Fig. 1b shows representative TEM images of unstained and negatively stained AFt-PbS nanocomposites. We note that the deposition of aqueous AFt-PbS on hydrophobic TEM grid can lead to the clustering of the nanocomposites and/or to the formation of characteristic drying patterns, as seen in the unstained TEM image (Fig. 1b). TEM images reveal an electron-dense central core (PbS), surrounded by an electron transparent protein shell with average diameter ~12 nm. The presence of the PbS nanocrystals inside AFt was confirmed by energy dispersive X-ray (EDX) analysis, which revealed characteristic Pb and S lines.

MTT [3-(4,5-dimethylthiazol-2-yl)-2,5-diphenyltetrazolium bromide] viability assays were performed to determine the growth inhibitory effects of AFt-PbS nanocomposites in CRC cells. Following 72 h exposure, consistent dose dependent growth inhibition was observed in HCT116 and HT29 CRC cell

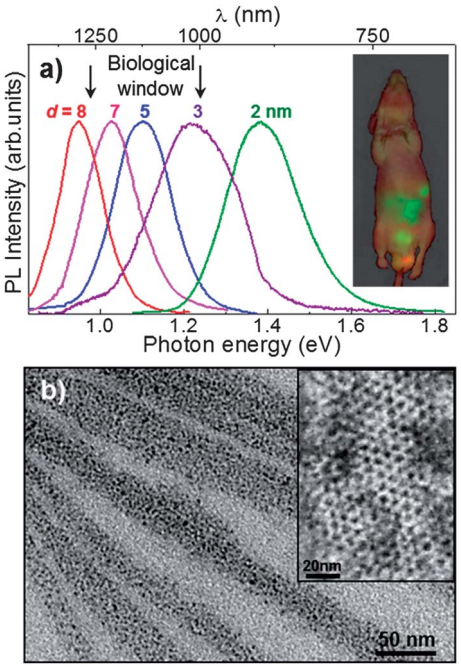

Fig. 1 (a) Room temperature PL spectra of PbS QDs with different sizes. Inset: the PL of PbS solution injected in mice through the peritoneal cavity. (b) TEM images of unstained AFt-PbS and (inset) negatively stained with uranyl acetate.

lines (Fig. 2a). Following initial seeding at 3×10^3 cells per well, mean growth inhibition by 50%, GI_{50}, values of ~70 μg mL^{-1} were obtained for both cell lines with standard error of mean

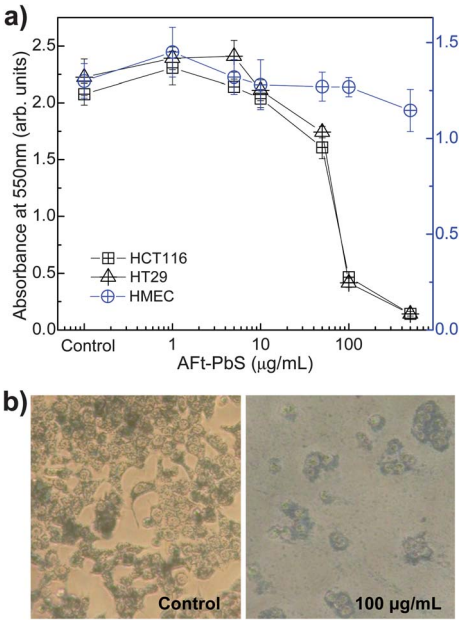

Fig. 2 (a) MTT results of normal cells (HMEC-1) and cancerous cell lines (HCT116, HT29) following treatment with AFt-PbS for 72 h. Mean ± SD of representative experiments are shown ($n = 8$); experiments were performed ≥3×. (b) Light microscopy images of HCT116 cells not exposed to AFt-PbS (left image) and following 72 h treatment with 100 mg per mL of AFt-PbS (right image). Formazan crystals formed by cellular metabolism of MTT can be observed. Images acquired with magnification ×20.

(SEM) <5%. Increasing the initial seeding density (in effect reducing the AFt-PbS QD concentration available per cell) did not impact on growth inhibition. In fact, at higher seeding densities (5×10^3, 1×10^4), exposure to AFt-PbS at concentrations >GI_{50} values evoked total growth inhibition (TGI) and cytotoxicity; TGI and LC_{50} (concentration which killed 50% cells treated) values <200 μg mL^{-1} were observed following 72 h exposure in HCT116 cells seeded at 10^4 per well (data not shown). Images of HCT116 cells were captured prior to formazan solubilization. Control cells revealed ~75% confluence, adhering to their plastic support in a pavement mosaic pattern. They were rich in formazan crystals, reflecting metabolism of MTT by healthy viable cells (Fig. 2b). In contrast, cells exposed for 72 h to 100 μg mL^{-1} of AFt-PbS QDs were markedly fewer in number (~80% less than in control wells). Although retaining the ability to metabolize MTT to formazan, cells displayed morphological features characteristic of programmed cell death (apoptosis): cytoplasmic shrinkage as a consequence of cytoskeletal protein cleavage, reduced metabolic capacity and loss of membrane integrity (Fig. 2b). AFt alone (≤1 mg mL^{-1}) had no effect on proliferation as evidenced by MTT metabolism and cell morphology. Thus, the PbS nanocrystals were responsible for growth inhibition of CRC cells.

To gain understanding of any potential therapeutic window and estimate the risks of AFt-PbS QDs towards normal tissues, we evaluated their effects on human dermal microvessel endothelial cells (HMEC-1). Following 72 h exposure of cells to AFt-PbS QDs, MTT assays disclosed mean GI_{50} values ~800 μg mL^{-1}; >10-fold greater resistance compared to CRC cells (Fig. 2). These data corroborate our previous work demonstrating that MRC5 fibroblasts were >5-fold resistant to AFt-PbS QDs than breast cancer cells.[19]

In the wake of MTT assay results we sought to identify more specifically the effects of 70 μg mL^{-1} and 140 μg mL^{-1} (GI_{50} and 2× GI_{50} values respectively) AFt-PbS on CRC cells. We investigated cell cycle perturbations by flow cytometry. The DNA content of individual cells (>10 000) within a given population was analyzed and the cell cycle profile reconstructed. Cell cycle histograms of untreated cells reveal characteristic logarithmic growth profiles: distinct cell cycle phases according to DNA content (see for example the typical cell cycle profile for control HT29 cells in Fig. 3a). Following 72 h exposure of CRC to GI_{50} and 2× GI_{50} values AFt-PbS, cell cycle profiles changed dramatically. Fig. 3a also illustrates the cell cycle profile of HT29 cells exposed to 140 μg mL^{-1} AFt-PbS. Analyses revealed >40% and >70% events in the pre-G1 compartment for both HCT116 and HT29 CRC cell lines, following exposure to 70 and 140 μg mL^{-1} AFt-PbS (Fig. 3b). Pre-G1 occupancy represents sub-diploid events consistent with apoptosis-associated DNA fragmentation: a consequence of caspase activity. Caspases are cysteine-dependent aspartate-directed proteases that play a central role in cellular apoptosis.[27,28] Resistance to apoptosis is a major contributor to tumorigenesis and a recognized hallmark of cancer.[29] Thus, induction of apoptosis in cancer cells is an important goal of experimental cancer therapies.

To confirm the apoptotic nature of cell death, we performed dual Annexin V (AV)/propidium iodide (PI) staining and cell

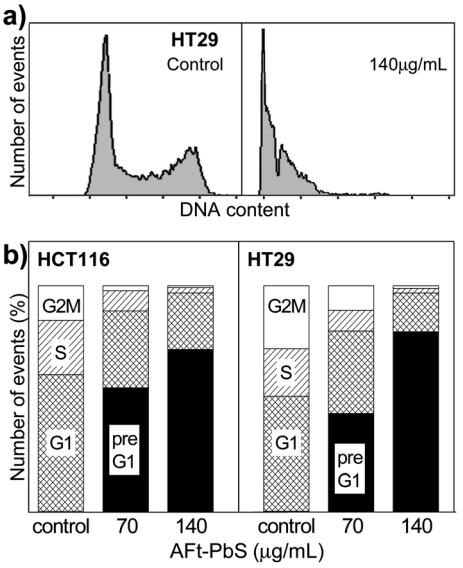

Fig. 3 (a) DNA histograms revealing effect of exposure of HT29 cells to 140 μg mL^{-1} AFt-PbS QDs for 72 h on the cell cycle profile. (b) Histograms showing HCT116 and HT29 CRC cell populations occupying different cell cycle stages following 72 h exposure of cells to 70 μg mL^{-1} or 140 μg mL^{-1} AFt-PbS; experiments were performed at least 3×; ≥10 000 events recorded from each trial.

population analysis by flow cytometry. AV binds to phosphatidylserine which becomes exposed on the outer leaflet of the cell membrane during the early stages of apoptosis, as cell membranes lose their asymmetry. Evaluation of CRC cells treated with AFt-PbS QDs revealed distinct AV positive (+), PI negative (−) and AV+, PI+ HCT116 and HT29 populations indicative of cells progressing through early- and late-stage apoptosis. To exemplify, Fig. 4 shows HCT116 cell population distribution following 72 h exposure to AFt-PbS: ~31% and ~23% of cells were observed undergoing early and late apoptosis, respectively, following exposure to 1× GI_{50} AFt-PbS QDs. These figures rose to ~48% and ~33% when cells were challenged with 2× GI_{50} value. Observations made in HCT116 CRC populations are summarized in Fig. 4b.

Exposure of HMEC-1 cells to 70 μg mL^{-1} and 140 μg mL^{-1} AFt-PbS QDs (≤72 h; experimental conditions which represent GI_{50} and 2× GI_{50} AFt-PbS concentrations in CRC cells) neither perturbed cell cycle nor induced apoptosis. The AFt protein cage (≤1 mg mL^{-1}) neither perturbed cell cycle nor induced apoptosis in any cell line studied (not shown), hence AFt[30,31] does not compromise cell viability. In cancer cells, increased ferritin (Ft) uptake and iron retention is mediated largely by enhanced TRs (as well as reduced iron export *via* ferroportin).[20] By exploitation of this property, encapsulation of QDs within a non-toxic AFt protein cage aims to minimize collateral toxicity associated with systemic therapy, promoting preferential receptor-mediated endocytosis of PbS nanocrystals by cancer cells. Significantly, HMEC-1 cells were less sensitive to growth inhibitory effects of AFt-PbS QDs compared to CRC cells ($p < 0.0001$; Student's t test). Thus the dual purpose AFt cage increases biocompatibility[32] and facilitates uptake by cancer cells.[24] Up-regulated TRs on the cell membrane of many cancer

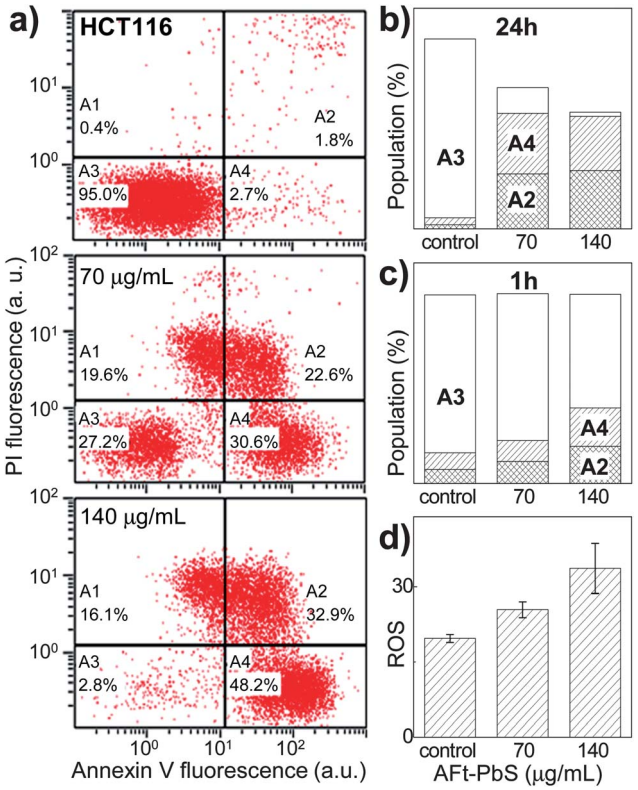

Fig. 4 (a) Typical population distribution of HCT116 cells (top) and the effect of 72 h exposure to AFt-PbS at concentrations of GI_{50} and 2× GI_{50}. A3, A4 and A2 correspond to viable, early and late apoptotic cell populations, respectively. A1 reveals the proportion of necrotic (or disintegrating apoptotic) cells. (b) Histograms of HCT116 cell populations following exposure to AFt-PbS for 72 h. (c) HCT116 apoptosis after 1 h exposure to AFt-PbS QDs. (d) ROS generation in HCT116 following exposure to AFt-PbS for 1 h.

cell types could be exploited for targeted delivery of therapeutic or imaging molecules to malignant cells, concurrently blocking iron transport, thus starving the cancer cell of iron.[33,34] Interestingly, following just 1 h exposure to AFt-PbS, subsequent growth of CRC cells was significantly inhibited. For both CRC cell lines studied, 1 h exposure led to dramatic decrease in cell proliferation with GI_{50} values of ~200–300 μg mL^{-1} (data not shown). Indeed, evaluation of the effect of treatment time has shown that just 1 h exposure of cells to 70 μg mL^{-1} and 140 μg mL^{-1} AFt-PbS proved sufficient to trigger apoptosis in CRC cells (Fig. 4c). Our data suggest that apoptotic cell death in CRC cells is induced *via* mechanisms which involve PbS-induced generation of reactive oxygen species (ROS). HCT116 cells challenged with AFt-PbS at concentrations of GI_{50} and 2× GI_{50} for 1 h revealed enhanced ROS (by 29% and 70%, respectively; Fig. 4d), compared to untreated cells.

Tumor cells generate elevated levels of ROS; further oxidative stress, tolerated by normal cells, will surpass the endurable threshold for cancer cells and induce apoptosis.[35,36] Experimental and clinical cancer therapies attempt to exploit this difference between normal and cancer cells to deliver effective selective treatment. However, both cytotoxicity and cardiotoxicity of the anthracycline antibiotic doxorubicin, administered in treatment for many cancers, is linked to time- and dose-dependent ROS generation.[37] 5-Fluoruracil, the standard of care in CRC has been reported to induce widespread (rather than cancer cell-specific) apoptosis through intracellular oxidative stress.[38–40]

Next we examined whether single CRC cells could survive AFt-PbS QDs challenge and proliferate to form progeny colonies, indicative of the ability to repopulate a tumor.[41] HCT116 and HT29 cells were exposed for 24 h to 140, 70, 35, 14 and 7 μg mL^{-1} AFt-PbS QDs (representing 2×, 1×, 0.5×, 0.2× and 0.1× GI_{50} values). Media containing nanocomposites were then removed and cells washed thoroughly and gently before addition of fresh nutrient medium. Clonogenic assay results were stark and unequivocal; CRC colonies were unable to grow following 24 h exposure of cells to AFt-PbS QDs at concentrations corresponding to 2×, 1×, 0.5×, 0.2× and 0.1× GI_{50} values (Fig. 5). Evidence presented herein corroborates data previously reported that AFt-PbS QDs evoke cancer cell-specific apoptosis through elevation of ROS within breast cancer cells, following TR-mediated endocytosis.[19,24] It was therefore necessary to determine whether AFt-PbS QDs could be tolerated *in vivo*.

Acute toxicity tests were carried out in non-tumor-bearing female athymic mice and HCT116 tumor-bearing mice. Animals received 200 μL 5 mg mL^{-1} AFt PbS-QDs either by i.p. (intraperitoneal) or s.c. (subcutaneous) injection on 3 consecutive days (1, 2 and 3). AFt-PbS nanocomposites were well tolerated, and no toxic events were observed. Neither weight loss nor adverse behavioural and health indicators were observed throughout the duration of the 15 day study. Specifically, animals' activity, vocalization, expression, interaction with cage-mates and response to handling remained unaffected by treatment. Healthy skin and eye condition was maintained, no rash development, inflammation, infection, dehydration were observed. No abdominal swelling occurred, appetite, defecation and urination patterns remained unaffected. Post-mortem, no indications of acute toxicity were detected in livers, spleens, kidneys or peritonea. *In vivo* efficacy and detailed bio-distribution studies are on-going and may inform as to whether CRC tumors are amenable to AFt-PbS imaging and therapy.

In conclusion, AFt-PbS nanocomposites evoke cytotoxicity in CRC cell lines, triggering apoptosis *via* a mechanism which involves PbS-induced generation of ROS. Non tumorigenic

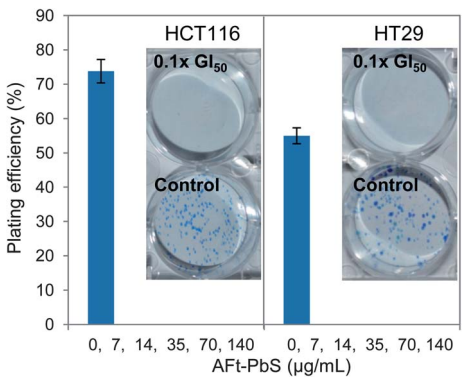

Fig. 5 CRC colony growth detected 7 days post 24 h exposure of CRC cells to AFt-PbS QDs. Colonies were fixed, stained with methylene blue and counted.

HMEC-1 cells were resistant to AFt-PbS QDs. Preliminary investigations in human pancreatic and ovarian carcinoma cell lines further confirm the cancer-cell selective nature of AFt-PbS induced growth inhibition. NIR photoluminescence of PbS QDs can be imaged *in vivo* and AFt-PbS are well tolerated by mice. Differential anticancer therapeutic activity combined with NIR photoluminescence may offer potential in cancer diagnosis, imaging and treatment. A pertinent and exciting research goal is to harness the theranostic potential of AFt-encapsulated multifunctional nanoparticles *in vivo*.

Experimental materials and methods

Sample preparation

PbS quantum dots were synthesized in aqueous solution by previously reported methods.[19,25] A Pb^{2+} precursor solution was prepared with 2.5×10^{-4} mol of lead acetate $Pb(CH_3COO)_2$, 1.5×10^{-3} mol of thioglycerol (TGL) and 5×10^{-4} mol of dithioglycerol (DTG) in 15 mL of deionized water, where the thiols act as capping agents. The pH of the solution was adjusted to a value of 11.0 by addition of triethylamine. Nanocrystal growth was completed by addition of a 0.1 M solution of sodium sulfide Na_2S at a molar ratio 1 : 0.3 of Pb to S. The synthesis was performed under N_2 flux and the resulting solutions were stored in a fridge at $T = 4$ °C under N_2 atmosphere. Apoferritin was obtained from horse spleen ferritin (purchased from Sigma Aldrich) by reductive dissolution of the iron oxide core. AFt-PbS was prepared using two alternative routes. In the first one, pH dependent reassembly of AFt was exploited to entrap preformed PbS nanocrystals within the AFt cavity. In the second, nanoreactor route, Pb^{2+} and S^{2-} ions entered the hollow AFt core through the channels; and PbS QDs were formed directly inside the AFt cavity.

Cell culture

Cell lines were purchased from the American Type Culture Collection (ATCC). Cells were cryopreserved (−155 °C in liquid nitrogen) and retrieved from the bank for cultivation at 37 °C in an atmosphere containing 5% CO_2. Cells were passaged twice weekly to maintain logarithmic growth and discarded after <20 passages to minimize phenotypic drift. CRC HCT116 and HT29 cells were cultured in RPMI-1640 nutrient medium supplemented with 10% fetal bovine serum (FBS). Human microvascular endothelial cells (HMEC-1) were cultured in EBM-2 medium supplemented with 10% FBS, epidermal growth factor (EGF; 10 μg L^{-1}) and hydrocortisone (1 mg L^{-1}). HCT116, HT29 and HMEC-1 cells were used in all studies.

Growth inhibitory assays

In vitro screening was carried out using the MTT [3-(4,5-dimethylthiazol-2-yl)-2,5-diphenyltetrazolium bromide] assay.[42] Cells were seeded into 96-well microtiter plates at a density of 3×10^3 per well and allowed 24 h to adhere before agents were introduced. A stock concentration of 5 mg mL^{-1} AFt-PbS QDs was maintained at 4 °C, protected from light. AFt-PbS was diluted in nutrient medium to final concentrations ranging from 1 μg mL^{-1} to 500 μg mL^{-1}; $n = 8$, immediately prior to cell treatment. Control wells received vehicle alone. Experimental plates were incubated at 37 °C for 72 h. Viable cells at the time of addition (time-zero T0), and following 72 h were determined by cell-mediated MTT reduction. MTT was added to each well at final concentration of 400 μg mL^{-1} and plates were incubated at 37 °C for 2 h to allow reduction of MTT by cellular dehydrogenases to insoluble purple formazan crystals. Well supernatants were aspirated and formazan was solubilized by addition of DMSO (150 μL per well). Absorbance at $\lambda = 550$ nm was measured by Anthos Labtec systems plate reader. The measured intensity is proportional to metabolic activity of cells and correlates to cellular viability. Performing MTT assays at the time of agent addition (T0) as well as after 72 h incubation, allows determination of agent concentration able to inhibit growth by 50% (GI_{50} values).

Cell cycle analyses

Cells were seeded in 6 well plates at a density of 5×10^4 per well and incubated overnight prior to AFt-PbS QD addition. Following treatment, cells were harvested, washed (PBS; 4 °C) and centrifuged (1200 rpm; 5 min; 4 °C). Cells were then resuspended in fluorochrome solution (50 μg mL^{-1} propidium iodide (PI), 0.1 mg mL^{-1} ribonuclease A, 0.1% sodium citrate and 0.1% Triton-X-100). Samples were transferred to Facs tubes, protected from light and stored at 4 °C overnight. Cell cycle analyses were performed using a Beckman Coulter EPICS-XL flow cytometer. Data were evaluated using EXPO32 software.

Annexin-V assay

Cells were seeded at 5×10^4 in 6 well plates and then treated with AFt-PbS QDs after overnight agent-free incubation. Following desired exposure, cells were collected, washed in ice cold PBS and transferred, with medium and detached cells, to Facs tubes. Following centrifugation (1200 rpm; 5 min; 4 °C), supernatants were discarded and cells resuspended in 1 mL fresh medium. For each sample, cells were counted using a hemocytometer, and 1×10^5 cells transferred to a fresh Facs tube containing 1 mL ice cold PBS. Following centrifugation, 100 μL Annexin-V buffer (10 mM HEPES (pH 7.4), 0.14 M NaCl, 2.5 mM $CaCl_2$) and 5 μL Annexin-V–FITC (Santa Cruz, CA) were added. Samples were incubated in the dark at room temperature for 15 min before further addition of 400 μL Annexin-V buffer and 10 μL 50 μg mL^{-1} PI in PBS. Samples were placed at 4 °C in the dark for 10 min, then analyzed using a Beckman Coulter EPICS-XL flow cytometer.

Clonogenic assays

Cells (200 HCT116 or 250 HT29 cells per well) were seeded into 6-well plates and allowed to attach overnight. AFt-PbS was introduced at final concentrations 140, 70, 35, 14 and 7 μg mL^{-1} corresponding to 2×, 1×, 0.5×, 0.2× and 0.1× GI_{50} value. Following 24 h treatment, medium and QDs were removed, cells were washed twice in 1 mL PBS and 2 mL fresh nutrient medium was introduced into wells. Plates were placed in the incubator and colonies were allowed to form until >50 cells per

colony were visible in control wells (6–7 days). Medium was aspirated from wells and colonies were washed twice with 1 mL ice cold PBS, before being fixed in 100% MeOH for 10 min. Colonies were stained using 0.5 mL 0.05% methylene blue in 1 : 1 dH_2O–MeOH. Colonies were rinsed 3-times in tap water, air dried and counted.

Detection of reactive oxygen species

Cells were seeded in 6-well plates at a density of 5×10^4 cells per well in 2 mL medium and allowed to attach overnight before introduction of AFt-PbS. During the final 30 min of the desired exposure period, H_2DCFDA (final concentration 5 μM) was added to each well. Floating and attached cells were pooled and pelleted by centrifugation (1200 rpm, 5 min, 4 °C). Supernatant was discarded and cells resuspended and washed in 1 mL ice cold PBS before centrifugation to pellet the cells. This process was repeated before addition of 0.5 mL PI at a concentration 10 μg mL^{-1} in PBS to each sample. Samples were protected from light and incubated on ice for 10 min and were analyzed within 1 h on a Beckman Coulter Epics XL-MCL flow cytometer.

Imaging and acute toxicity studies

All *in vivo* studies were conducted under the UK Home Office Licence number PPL 40/3559. UKCCCR guidelines for the welfare of animals were strictly adhered to throughout. NCRI guidelines for the welfare and use of animals in cancer research, LASA good practice guidelines and FELAS working group on pain and distress guidelines were also followed. Preclinical toxicology studies were conducted in compliance with UK GLP standards (Schedule 1, Good Laboratory Regulations 1999 (SI 1999/3106)). Animals received AFt-PbS either i.v. or i.p. (200 μL delivering 1 mg PbS) on days 1, 2 and 3. Mice were imaged on days 1 and 3 directly after treatment and again on day 15. Weights and behaviour of mice were recorded throughout the 15 day experimental period.

Acknowledgements

This work was supported by The University of Nottingham and the Medical Research Council (MRC). SM and ML thank ERC (Advanced Grant) for financial support. The authors thank Alison Ritchie for technical expertise and useful discussions.

References

1 World Cancer Research Fund International, www.wcrf.org/cancer_statistics/cancer_facts.
2 R. Labianca, M. A. Pessi and G. Zamparelli, *Drugs*, 1997, **53**, 593.
3 J. Y. Douillard, *Lancet*, 2000, **355**, 1372.
4 M. L. Rothenberg, *Oncologist*, 2001, **6**, 66.
5 A. Schroeder, D. A. Heller, M. M. Winslow, J. E. Dahlman, G. W. Pratt, R. Langer, T. Jacks and D. G. Anderson, *Nat. Rev. Cancer*, 2012, **12**, 39.
6 S. Kaur, G. Venktaraman, M. Jain, S. Senapati, P. K. Garg and S. K. Batra, *Cancer Lett.*, 2012, **315**, 97.
7 M. E. Davis, Z. Chen and D. M. Shin, *Nat. Rev. Drug Discovery*, 2008, **7**, 771.
8 D. K. Kirui, D. A. Rey and C. A. Batt, *Nanotechnology*, 2010, **21**, 105105.
9 J. W. Shao, R. J. Griffin, E. I. Galanzha, J. W. Kim, N. Koonce, J. Webber, T. Mustafa, A. S. Biris, D. A. Nedosekin and V. P. Zharov, *Sci. Rep.*, 2013, **3**, 1293.
10 Y. L. Yu, L. R. Xu, J. Chen, H. Y. Gao, S. Wang, J. Fang and S. K. Xu, *Colloids Surf., B*, 2012, **95**, 247.
11 M. Gazouli, A. Lyberopoulou, P. Pericleous, S. Rizos, G. Aravantinos, N. Nikiteas, N. P. Anagnou and E. P. Efstathopoulos, *World J. Gastroenterol.*, 2012, **18**, 4419.
12 C. Yang, C. X. Xu, X. M. Wang and X. Hu, *Analyst*, 2012, **137**, 1205.
13 A. M. Smith, M. C. Mancini and S. M. Nie, *Nat. Nanotechnol.*, 2009, **4**, 710.
14 X. Y. Liu, W. Wei, S. J. Huang, S. S. Lin, X. Zhang, C. M. Zhang, Y. G. Du, G. H. Ma, M. Li, S. Mann and D. Ma, *J. Mater. Chem. B*, 2013, **1**, 3136.
15 S. Mann, *Nat. Mater.*, 2009, **8**, 781.
16 J. C. Cutrin, S. G. Crich, D. Burghelea, W. Dastru and S. Aime, *Mol. Pharmaceutics*, 2013, **10**, 2079.
17 R. M. Xing, X. Y. Wang, C. L. Zhang, Y. M. Zhang, Q. Wang, Z. Yang and Z. J. Guo, *J. Inorg. Biochem.*, 2009, **103**, 1039.
18 F. Yan, Y. Zhang, H. K. Yuan, M. K. Gregas and T. Vo-Dinh, *Chem. Commun.*, 2008, 4579.
19 L. Turyanska, T. D. Bradshaw, J. Sharpe, M. Li, S. Mann, N. R. Thomas and A. Patanè, *Small*, 2009, **5**, 1738.
20 S. V. Torti and F. M. Torti, *Nat. Rev. Cancer*, 2013, **13**, 342.
21 K. C. Gatter, G. Brown, I. S. Trowbridge, R. E. Woolston and D. Y. Mason, *J. Clin. Pathol.*, 1983, **36**, 539.
22 H. Shinohara, D. Fan, S. Ozawa, S. J. Yano, M. Van Arsdell, J. L. Viner, R. Beers, I. Pastan and I. J. Fidler, *Int. J. Oncol.*, 2000, **17**, 643.
23 C. M. Hessel, V. P. Pattani, M. Rasch, M. G. Panthani, B. Koo, J. W. Tunnell and B. A. Korgel, *Nano Lett.*, 2011, **11**, 2560.
24 L. Turyanska, T. D. Bradshaw, M. Li, P. Bardelang, W. C. Drewe, M. W. Fay, S. Mann, A. Patanè and N. R. Thomas, *J. Mater. Chem.*, 2012, **22**, 660.
25 B. Hennequin, L. Turyanska, T. Ben, A. M. Beltran, S. I. Molina, M. Li, S. Mann, A. Patanè and N. R. Thomas, *Adv. Mater.*, 2008, **20**, 3592.
26 L. Turyanska, U. Elfurawi, M. Li, M. W. Fay, N. R. Thomas, S. Mann, J. H. Blokland, P. C. Christianen and A. Patanè, *Nanotechnology*, 2009, **20**, 315604.
27 G. M. Cohen, *Biochem. J.*, 1997, **326**(1), 1.
28 R. U. Janicke, M. L. Sprengart, M. R. Wati and A. G. Porter, *J. Biol. Chem.*, 1998, **273**, 9357.
29 D. Hanahan and R. A. Weinberg, *Cell*, 2011, **144**, 646.
30 L. Zhang, W. Fischer, E. Pippel, G. Hause, M. Brandsch and M. Knez, *Small*, 2011, **7**, 1538.
31 L. Li, C. J. Fang, J. C. Ryan, E. C. Niemi, J. A. Lebron, P. J. Bjorkman, H. Arase, F. M. Torti, S. V. Torti, M. C. Nakamura and W. E. Seaman, *Proc. Natl. Acad. Sci. U. S. A.*, 2010, **107**, 3505.
32 X. Liu, W. Wei, Q. Yuan, X. Zhang, N. Li, Y. Du, G. Ma, C. Yan and D. Ma, *Chem. Commun.*, 2012, **48**, 3155.

33 T. R. Daniels, E. Bernabeu, J. A. Rodriguez, S. Patel, M. Kozman, D. A. Chiappetta, E. Holler, J. Y. Ljubimova, G. Helguera and M. L. Penichet, *Biochim. Biophys. Acta, Gen. Subj.*, 2012, **1820**, 291.

34 T. R. Daniels, T. Delgado, G. Helguera and M. L. Penichet, *Clin. Immunol.*, 2006, **121**, 159.

35 B. Zhu, X. Li, Y. Zhang, C. Ye, Y. Wang, S. Cai, H. Huang, Y. Cai, S. Yeh, Z. Huang, R. Chen, Y. Tao and X. Wen, *Int. J. Cancer*, 2013, **132**, 2270.

36 M. Nagai, N. H. Vo, L. Shin Ogawa, D. Chimmanamada, T. Inoue, J. Chu, B. C. Beaudette-Zlatanova, R. Lu, R. K. Blackman, J. Barsoum, K. Koya and Y. Wada, *Free Radical Biol. Med.*, 2012, **52**, 2142.

37 Z. Fu, J. B. Guo, L. Jing, R. S. Li, T. F. Zhang and S. Q. Peng, *Toxicol. In Vitro*, 2010, **24**, 1584.

38 M. Lamberti, S. Porto, M. Marra, S. Zappavigna, A. Grimaldi, D. Feola, D. Pesce, S. Naviglio, A. Spina, N. Sannolo and M. Caraglia, *J. Exp. Clin. Cancer Res.*, 2012, **31**, 60.

39 S. Numazawa, K. Sugihara, S. Miyake, H. Tomiyama, A. Hida, M. Hatsuno, M. Yamamoto and T. Yoshida, *Basic Clin. Pharmacol. Toxicol.*, 2011, **108**, 40.

40 T. Matsunaga, Y. Tsuji, K. Kaai, S. Kohno, R. Hirayama, D. H. Alpers, T. Komoda and A. Hara, *Cancer Chemother. Pharmacol.*, 2010, **66**, 517.

41 N. A. Franken, H. M. Rodermond, J. Stap, J. Haveman and C. van Bree, *Nat. Protoc.*, 2006, **1**, 2315.

42 T. D. Bradshaw, E. L. Stone, V. Trapani, C. O. Leong, C. S. Matthews, R. te Poele and M. F. Stevens, *Breast Cancer Res. Treat.*, 2008, **110**, 57.